Distinct Photocurrent Response of Individual GaAs Nanowires Induced by n-Type Doping

Hui Xia,[†] Zhen-Yu Lu,[†] Tian-Xin Li,[†,*] Patrick Parkinson,[§] Zhi-Ming Liao,[∥] Fu-Hao Liu,[‡] Wei Lu,[†,*] Wei-Da Hu,[†] Ping-Ping Chen,[†] Hong-Yi Xu,[∥] Jin Zou,[∥,⊥] and Chennupati Jagadish[§]

[†]National Laboratory for Infrared Physics, and [‡]Key Laboratory of Infrared Imaging Materials and Detectors, Shanghai Institute of Technical Physics, Chinese Academy of Sciences, 500 YuTian Road, Shanghai 200083, People's Republic of China, [§]Department of Electronic Materials Engineering, Research School of Physics and Engineering, The Australian National University, ACT, Canberra, 0200, Australia, and [∥]Materials Engineering and [⊥]Centre for Microscopy and Microanalysis, The University of Queensland, St Lucia, QLD 4072, Australia

ABSTRACT

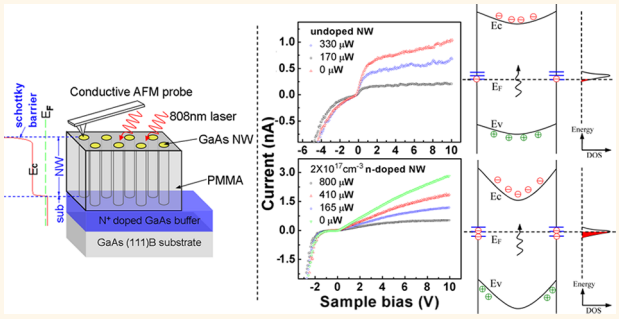

The doping-dependent photoconductive properties of individual GaAs nanowires have been studied by conductive atomic force microscopy. Linear responsivity against the bias voltage is observed for moderate n-doped GaAs wires with a Schottky contact under illumination, while that of the undoped ones exhibits a saturated response. The carrier lifetime of a single nanowire can be obtained by simulating the characteristic photoelectric behavior. Consistent with the photoluminescence results, the significant drop of minority hole lifetime, from several hundred to subpicoseconds induced by n-type doping, leads to the distinct photoconductive features. Moreover, by comparing with the photoelectric behavior of AlGaAs shelled nanowires, the equivalent recombination rate of carriers at the surface is assessed to be $>1 \times 10^{12}$ s^{-1} for 2×10^{17} cm^{-3} n-doped bare nanowires, nearly 30 times higher than that of the doping-related bulk effects. This work suggests that intentional doping in nanowires could change the charge status of the surface states and impose significant impact on the electrical and photoelectrical performances of semiconductor nanostructures.

KEYWORDS: GaAs nanowire · photoconductive property · intentional doping · minority carrier lifetime · surface states · photoelectric device

Semiconductor nanowires (NWs) have received increasing attention for their potential application in various fields. In particular, considerable progress has been achieved in NW-based optoelectronic devices such as photodetectors[1−5] and solar cells.[6−9] In principle, the performance of these devices is dominated by three factors: the efficiency of light absorption, the mobility, and the lifetime of carriers.[10] While the former one reflects the effective ratio of light harvesting, the latter two determine the collection efficiency of the photogenerated carriers and the intrinsic gain.[11] By taking advantage of the light funneling effect of vertically aligned NWs surrounded by low refractive index material, devices with a physical filling factor of only a few percent can effectively absorb the incident light,[10,12−14] achieving higher efficiency than thin film counterparts.[13] At the same time, the electron mobility of NWs is approaching the bulk value with the scattering effects essentially suppressed.[15−17] Very recently, the hole mobility in GaAs/AlGaAs NWs was reported to be similar to the best value observed in modulation-doped quantum wells.[18] While these findings prove the unique superiority of NWs in photoelectric conversion, the carrier lifetime is likely to hamper the pursuing of sensitive photodetection and efficient solar energy collection in NW-based devices.[19−21] According to the time-resolved spectroscopic studies, the carrier lifetime in NWs could be 2−3 orders shorter than that in the bulk case due to the impact of high density of surface traps,[15] and the way to improve the lifetime by overcoating the wires with barrier shells has also been discussed.[22,23] Notwithstanding these ongoing studies of carrier dynamics, direct demonstration of the influence of carrier lifetime on NWs' photoconductive response is still lacking, especially for the case of single wires.

Intentional doping in NWs with n- or p-type impurities is a key process to realize various functionalities.[7,24−28] Meanwhile, a high density of surface states, up to 10^{12} eV^{-1} cm^{-2}, for III−V NWs has been reported.[29,30] Considering that the carriers tend to fill the

* Address correspondence to txli@mail.sitp.ac.cn, luwei@mail.sitp.ac.cn.

Received for review March 3, 2012 and accepted June 22, 2012.

Published online June 22, 2012
10.1021/nn300962z

surface states, the consequence of doping on NWs' electrical properties could be different from the bulk case due to their high surface-to-volume ratio. Very recently, it has been reported that the trapping and release of carriers by surface states may cause a decline of the response time, which is critical for the application of NWs on high-speed devices.[5] Therefore, it is essential to detect the doping-related photoelectrical properties of NWs and go one step further to explore the underlying physical mechanism for NWs' application in photodetectors and solar cells.

In this study, the photoresponse of individual epitaxial GaAs NWs with different n-doping levels is characterized by conductive atomic force microscopy (conductive-AFM) under illumination. In contrast to that of the undoped wires, the photocurrent of NWs with a doping concentration higher than 2×10^{17} cm^{-3} exhibits an unusual linear relationship against the reverse bias voltage of the AFM tip–NW Schottky contact. This fact, together with the significant reduction of interband recombination revealed by a photoluminescence study, suggests that the n-type doping will lead to a dramatic drop of carrier lifetime in NWs. According to numerical simulation, the hole lifetime in the bare GaAs NWs is shortened from hundreds of picoseconds to less than 1 ps with doping concentration higher than 2×10^{17} cm^{-3}. In contrast to the impurity and defect effects inside NWs, the charging of surface states by n-type doping is inferred to play the essential role in depressing hole lifetime to subpicoseconds and results in the linear photoresponse of GaAs NWs. The study, for the first time, reveals the dependence of the surface traps on the density of majority carriers and derives the carrier lifetime in individual NWs based on their photoelectric behaviors.

RESULTS AND DISCUSSION

Structure of Nanowires. As listed in Table 1, GaAs NWs with four types of doping conditions are grown for comparison; also, two GaAs/AlGaAs/GaAs core–shell NW samples are prepared to evaluate the possible bulk effects of n-type doping on the NW's photoelectric property. High V–III flux ratio and low temperature are adapted to achieve efficient n-type doping in NWs on GaAs (111)B substrate during molecular beam epitaxial

TABLE 1. Description of Nanowire Structures and Doping Features

sample ID	NW structure	nominal concentration of n-type doping
u	bare GaAs NWs	unintentionally doped
n1	bare GaAs NWs	1×10^{16} cm^{-3}
n2	bare GaAs NWs	2×10^{17} cm^{-3}
n3	bare GaAs NWs	6×10^{17} cm^{-3}
cs-u	GaAs/AlGaAs/GaAs core–shell NWs	unintentionally doped
cs-n2	GaAs/AlGaAs/GaAs core–shell NWs	2×10^{17} cm^{-3} n-doped in GaAs core

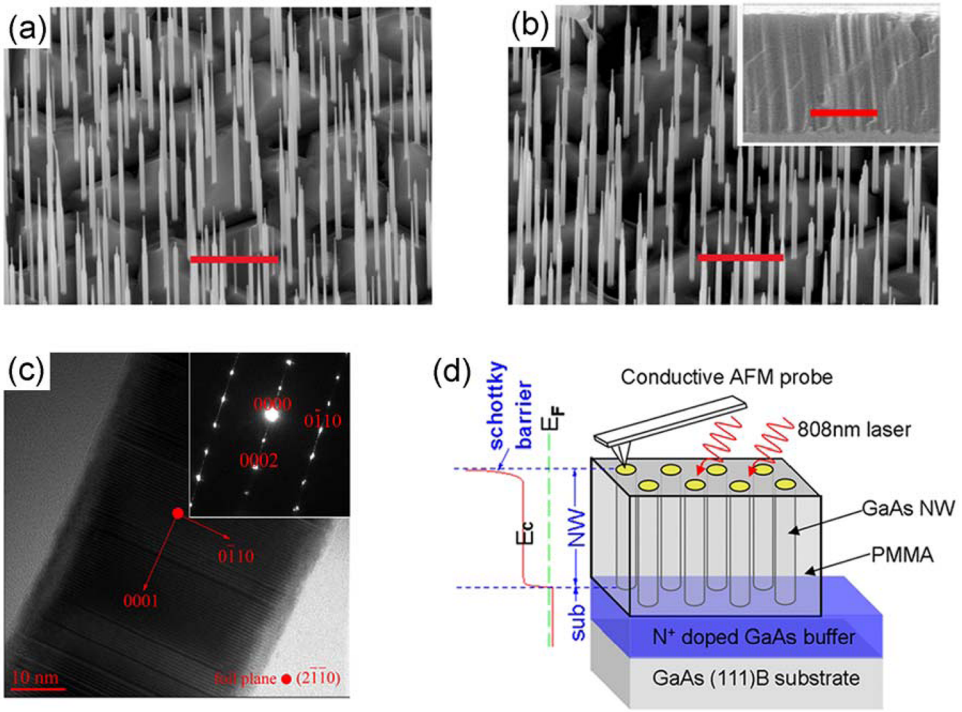

Figure 1. SEM images of Au-catalyzed MBE grown unintentionally doped (a) and 2×10^{17} cm^{-3} n-doped GaAs NWs (b). Inset in (b) is the SEM sectional image of the NW sample after it is coated with PMMA and polished. The scale bars in (a) and (b) represent 2 μm. (c) TEM image of unintentionally doped GaAs NW. Inset: Selected area electron diffraction of the NW. (d) Schematic experimental setup of photoconductive measurement on individual NWs with the band alignment illustrated on the left.

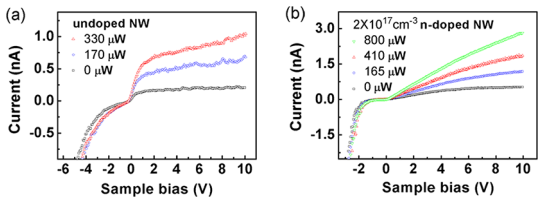

Figure 2. Photoconductive $I-V$ curves of individual NWs under illumination of different intensities: (a) unintentionally doped GaAs NWs; (b) 2×10^{17} cm^{-3} n-doped GaAs NWs.

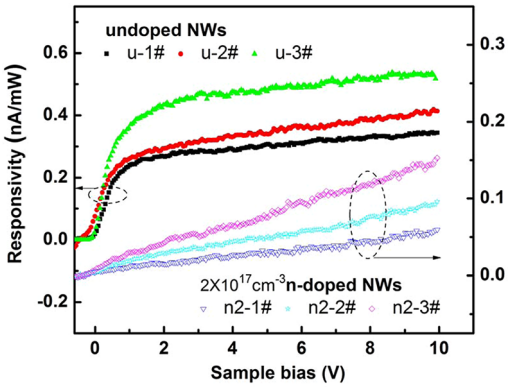

Figure 3. Normalized photoresponsivity of individual NWs. Three undoped NWs are labeled as u-1#, u-2#, and u-3# and three 2×10^{17} cm^{-3} n-doped GaAs NWs are labeled as n2-1#, n2-2#, and n2-3#.

(MBE) growth.[31] The NWs are typically 80−120 nm in diameter and 5−7 μm in height as seen in their scanning electron microscopy (SEM) images in Figure 1a,b. The crystal structure of NWs is hexagonal wurtzite within the our doping range, although lattice defects are occasionally observed by transmission electron microscopy (see Figure 1c and Figure S1 in Supporting Information for TEM results of nanowires with all doping conditions).

Doping Related Photoelectric Behavior of Nanowires. As sketched in Figure 1d, the photoelectrical property of individual NWs is measured by introducing laser light at 808 nm to the tip engaged area in conductive-AFM. Figure 2a,b plots the typical $I-V$ curves measured on individual undoped and 2×10^{17} cm^{-3} n-doped GaAs NWs, respectively, under illumination of different intensities with a spot size of ~5 mm. With no intentional excitation, the $I-V$ curves of NWs in both doping conditions exhibit rectifying character of the tip−wire Schottky contacts, as illustrated in Figure 1d.[32,33] Under reverse bias corresponding to the positive sample bias, a current of tens to a few hundreds of picoamperes is observed on all of the NWs mainly due to background excitation by the stray light of the AFM cantilever laser.[34]

While the photocurrent of the undoped NWs saturates after a rapid increase against the reverse bias as is commonly expected in a metal−semiconductor−metal (MSM) detector,[35,36] the counterparts of the doped ones show a more linear manner. This unusual behavior is confirmed by the bias-dependent photoresponsivity test

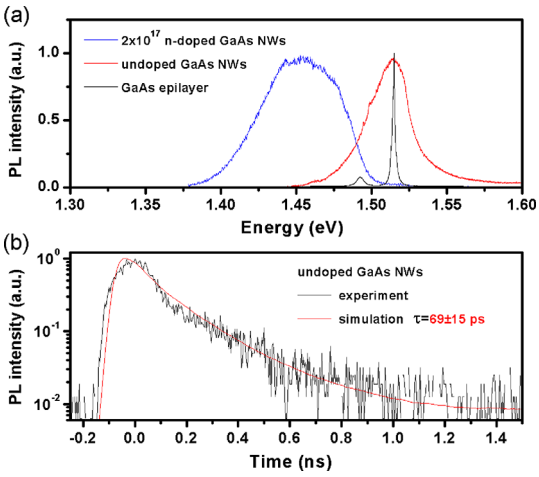

Figure 4. Photoluminescence of an ensemble of GaAs NWs at 4.5 K. (a) Normalized photoluminescence spectra of the undoped (red line), 2×10^{17} cm^{-3} n-type doped (blue line) GaAs NWs, and the epilayer (black line). (b) Time-resolved photoluminescence of the undoped GaAs NWs (black line) measured at the peak emission. The red line is a fitted response corresponding to an exponential decay of lifetime 69 ± 15 ps, convoluted with the instrument response function of the system.

on a number of NWs with some of the results shown in Figure 3. As can be noted, the responsivity discrepancy of NWs on the same sample can be several times in magnitude under identical measuring conditions. At the same time, the undoped NWs tend to yield higher responsivity than the n-type doped NWs though inconsistency of effective excitation intensity may exist in different samples. Moreover, the linear increase of the photoconductive response along with bias voltage suggests that different mechanisms dominate the relaxation and collection of photocarriers in the 2×10^{17} cm^{-3} n-type doped NWs.

Doping Related Photoluminescent Properties. Photoluminescence (PL) studies may provide further information to understand the carrier dynamics in NWs. As shown in Figure 4a, the low-temperature PL emission of an ensemble of undoped GaAs NWs peaks at the free exciton energy of 1.51 eV, which is consistent with that of the GaAs epilayer. Meanwhile, the spectrum of the 2×10^{17} cm^{-3} n-doped GaAs NWs shows a rather broadened peak around 1.45 eV with the exciton emission drastically diminished. The quenching of the interband recombination implies that some much faster process associated with n-type doping dominates the relaxation of the photocarriers, thus leading to a great reduction of carrier lifetime compared with that in the undoped GaAs NWs. This finding is partially supported by time-resolved photoluminescence (TRPL). By fitting the PL decay transient with a reconvoluted biexponential

$$\mathrm{PL}(t) = [A\exp(-t/\tau_1) + B\exp(-t/\tau_2)] \otimes \mathrm{IRF} \quad (1)$$

the exciton lifetime can be extracted. As shown in Figure 4b, upon fitting, τ_1 and τ_2 are decay constants of 69 ps and 2 ns, A and B are the relative amplitudes

(where $A/B \approx 100$, indicating a dominant short time scale), and IRF is the experimentally measured instrument response function. While the exciton lifetime is fitted as 69 ± 15 ps for the undoped GaAs NWs according to the transient PL results, no reliable information can be acquired in the n-doped GaAs NWs within the sensitivity or resolution of the equipment, suggesting a substantially shorter carrier lifetime.

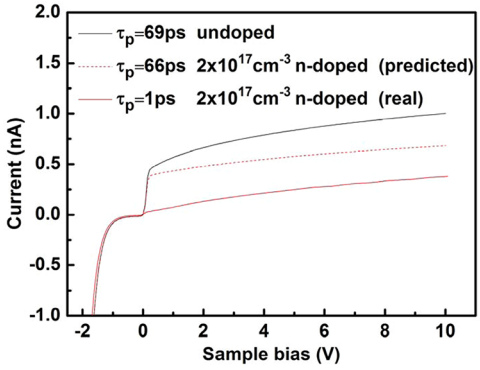

Figure 5. Calculated photo-*IV* curves of undoped NW for $\tau_p = 69$ ps (black solid line), 2×10^{17}cm^{-3} n-doped NW with $\tau_p = 66$ ps (red dashed line; the predicted photo-*IV* of 2×10^{17}cm^{-3} n-doped NW which takes into account the lifetime shortening, from 69 to 66 ps, induced by the SRH recombination), and the linear photo-*IV* of 2×10^{17}cm^{-3} n-doped NW is reproduced with τ_p set as 1 ps (red solid line).

Carrier Lifetime in Nanowires by Simulation. To investigate the influence of carrier lifetime on the photoconductive behavior of nanowires, a two-dimensional numerical model is established to simulate the current–voltage property of the AFM tip–NW setup under illumination (the details of the model are specified in the Methods section). We start from 69 ps for the minority hole lifetime in undoped GaAs NWs, the Schottky style photo-*IV* is well reproduced as shown in Figure 5. For 2×10^{17} cm^{-3} n-doped wires, the hole lifetime is slightly shortened to 66 ps for the Shockley–Read–Hall (SRH) recombination process, and the impurity scattering of carriers will degrade the photoelectric responsivity of the NWs. Even so, the simulated photo-*IV* curve of the n-doped NWs remains a

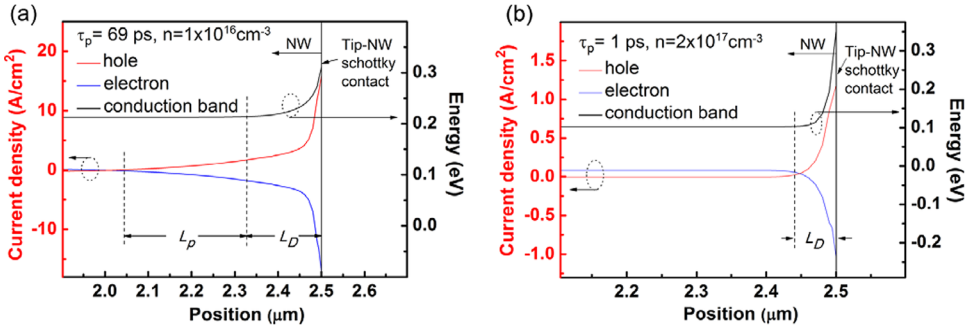

Figure 6. Simulated distribution of photocurrent density and conduction band alignment along the axial direction of NWs for different hole lifetime $\tau_p = 69$ ps (a) and $\tau_p = 1$ ps (b). L_D is the depletion width of Schottky barrier and L_p is the diffusion length of hole. The data is obtained at zero bias voltage. For $\tau_p = 69$ ps, the photogenerated holes in region L_D and L_p are effectively extracted. While for $\tau_p = 1$ ps, only holes in the Schottky barrier region (L_D) can be extracted.

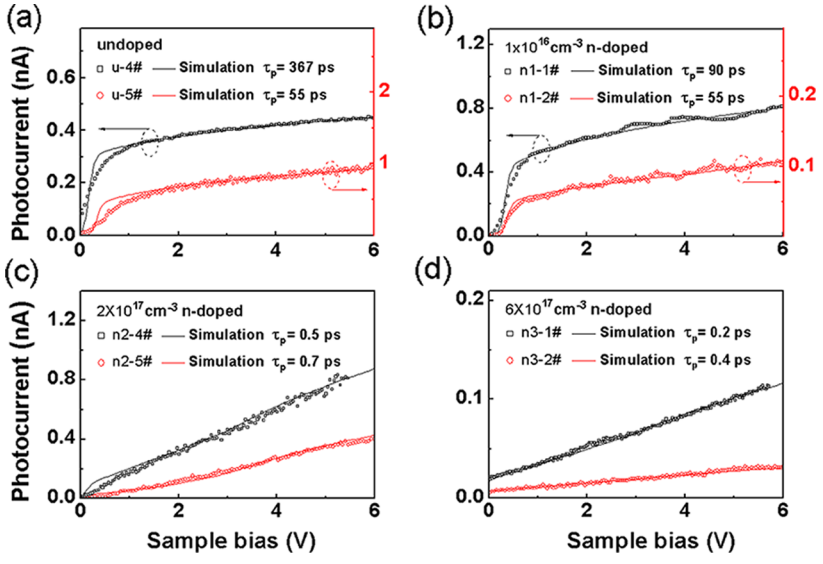

Figure 7. Experimental and simulated photocurrent *I*–*V* curves of (a) undoped, (b) 1×10^{16} cm^{-3}, (c) 2×10^{17} cm^{-3}, and (d) 6×10^{17} cm^{-3} n-doped GaAs NWs. In each plot, the red and black scatter lines represent the experimental results of two different NWs; the red and black solid lines are the corresponding fitting curves, from which the MHL of individual NW can be derived.

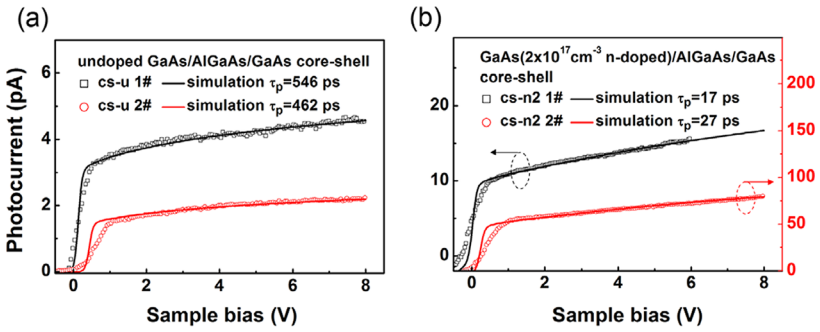

Figure 8. Experimental and simulated photocurrent *IV* curves of the GaAs/AlGaAs core−shell NWs with the GaAs core (a) undoped and (b) 2 × 10^{17} cm^{-3} n-doped. The large photocurrents of cs-n2 1# and cs-n2 2# NWs are coming from the high excitation power. In each plot, the red and black scatter lines represent the experimental results of two different NWs; the red and black solid lines are the corresponding fitting curves.

saturated mode. This indicates that, besides the influence of dopant impurities, n-type doping introduces further impact on the carrier dynamics in GaAs NWs. In fact, following the indication of dramatic reduction in PL, the linear photoconductive *I*−*V* curve can be numerically obtained when the hole lifetime is adjusted to 1 ps or less.

The simulation depicts the fading of Schottky character in photo-*IV*s of NWs with ultralow minority hole lifetime. Figure 6a,b gives the current density distribution of the electron and hole along the axial direction of the NWs with τ_p = 69 ps and τ_p = 1 ps, which represent the typical saturated and linear photoelectric responses, respectively. In both cases, the minority hole current contributes mostly to the photocurrent in the tip−NW junction region. The hole diffusion length is given by

$$L_p = \sqrt{D\tau_p} \quad (2)$$

where *D* is the diffusion coefficient of hole.[41] For τ_p = 69 ps (Figure 6a), L_p = 245 nm, considerably larger than the depletion length of Schottky barrier (L_D), then the total photocurrent is governed by the hole diffusion current, and it will saturate after the rapid counteraction of photovoltage. By contrast, L_p is 30 nm for τ_p = 1 ps (Figure 6b), in which case the drift current dominates the photocurrent:

$$\vec{J} = q\Delta n_p \mu_p \vec{\varepsilon} \quad (3)$$

where *q*, μ_p, and Δn_p are the charge, mobility, and the density of the photoexcited hole, respectively, and ε is the external electric field. This explains the linear photoconductive behavior in NWs with ultralow carrier lifetime, as the drift current is proportional to the external electric field.

Considering the relevance between photoelectric behavior and carrier lifetime of the nanowire, Figure 7 plots the experimental and simulated photocurrent curves of GaAs NWs with four different doping concentrations. The 1 × 10^{16} cm^{-3} doped NWs exhibit similar saturated behavior as the undoped ones, while the photocurrent of NWs with doping concentration higher than 2 × 10^{17} cm^{-3} shows a linear relationship against the positive sample bias. As mentioned before,

TABLE 2. Equivalent Recombination Rate of Minority Holes, $1/\tau_p$, in Nanowires with Different Structures and Doping Features

sample ID	NW structure	$1/\tau_p$ (s^{-1})
cs-u	undoped GaAs/AlGaAs/GaAs core−shell NWs	1 × 10^9−2 × 10^9
u	undoped bare GaAs NWs	5 × 10^9−20 × 10^9
cs-n2	GaAs(2 × 10^{17} cm^{-3} n-doped)/AlGaAs/GaAs core−shell NWs	3 × 10^{10}−7 × 10^{10}
n2	2 × 10^{17} cm^{-3} n-doped bare GaAs NWs	1 × 10^{12}∼2 × 10^{12}

the increase of photocurrent with the bias voltage is decided by hole diffusion length relative to the depletion width of the Schottky junction. Then the minority hole lifetime (MHL) of individual NWs can be extracted by fitting the experimental curves. As displayed in Figure 7a, the MHL of undoped GaAs NWs can deviate between 50 to several hundred picoseconds. It is considerably longer than the previously reported value of a few picoseconds observed in nominally undoped zinc-blende GaAs NWs.[15,22] The III−V wurtzite NWs are inferred to have different atomic and electronic structures on the surface compared to that of the zinc-blende ones,[37−39] which may be the clue to understand the discrepancy of carrier lifetime in NWs of two different types of crystal structures. For the lightly doped NWs, the MHL is reduced to less than 100 ps (Figure 7b). On the other hand, the numerical fitting reveals that the MHL of 2 × 10^{17} cm^{-3} doped NWs is about 0.5 ps (Figure 7c), while no significant further drop of MHL is found in the 6 × 10^{17} cm^{-3} doped NWs (Figure 7d). This is reasonable because the intraband relaxation time is of subpicosecond scale for photocarriers in GaAs.[40]

Bulk and Surface Effects on Carrier Lifetime by n-Type Doping. It is known that doping may degrade the optical and photoelectric properties by introducing contamination and lattice defects in semiconductors. On the other hand, surface effects are believed to play a prominent role in altering the dynamic feature of photocarriers in nanostructures with high surface-to-volume ratio.[19,20] By comparison with the photoelectric property of AlGaAs shelled nanowires, the contribution of bulk and surface effects of n-type doping on the drop of carrier lifetime can be

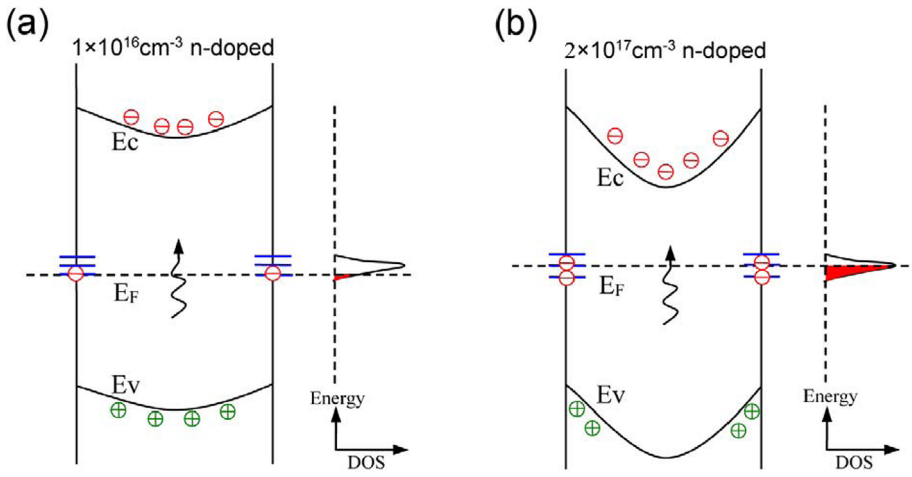

Figure 9. Schematic illustration of doping dependent surface status and carrier distribution under illumination in (a) 1×10^{16} cm^{-3}, and (b) 2×10^{17} cm^{-3} n-doped GaAs NWs. A high density of surface states (DOS) is assumed in the mid-band gap of wurtzite GaAs NW, and the Fermi level will thus be pinned. In contrast to the lightly doped NW, the acceptor-like centers at the surface (short blue line) are mostly occupied by electrons (red circle) due to the high doping concentration in 2×10^{17} cm^{-3} n-doped NWs and result in a high built-in field which accumulates the photoinjected holes (green circle) in the NW's surface.

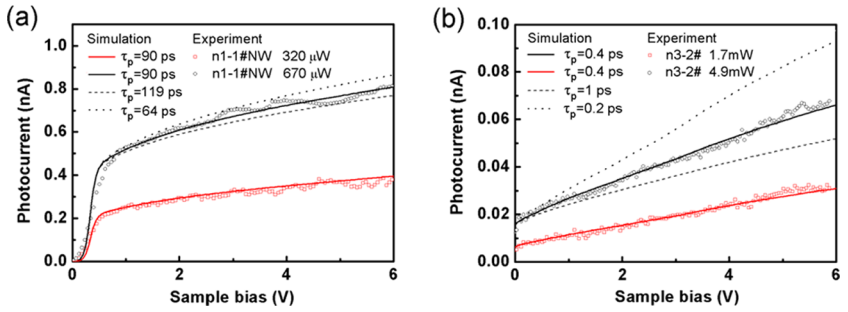

Figure 10. Fitting the photocurrent curves of a 1×10^{16} cm^{-3} n-doped NW (a), as well as that of a 6×10^{17} cm^{-3} n-doped NW (b) under different exciting intensities. The scattered lines are experimental data, while the solid, dashed, and dotted lines are the simulated curves with different minority hole lifetimes.

quantitatively determined. Figure 8 presents the experimental and simulated photo-*IV* curves of the GaAs/AlGaAs core–shell NWs with the GaAs core undoped and 2×10^{17} cm^{-3} n-doped. Unlike those of the bare GaAs NWs, the photo-*IV*s of all the wires with core–shell structures exhibit typically saturated behavior regardless the doping of the GaAs core; also, the simulated hole lifetimes are improved after capped with the AlGaAs shell. Both suggest that the negative influence of surface effects on the carrier lifetime is suppressed. The equivalent recombination rates of minority holes, defined as $1/\tau_p$, in NWs with different structures and doping conditions are calculated and shown in Table 2. The difference of recombination rates between the doped and undoped core–shell NWs represents the bulk effects of n-type doping; the value is about $3–7 \times 10^{10}$ s^{-1}, noticeably higher than the electron–hole radiative recombination rate in GaAs. On the other hand, the equivalent recombination rates of carriers in bare NWs can be $>1 \times 10^{12}$ s^{-1} for doping concentration $\geq 2 \times 10^{17}$ cm^{-3}, which implies that the recombination rate at the surface could be substantially larger than that inside the wires and thus causes the linear photoconductive behavior of tip–wire Schottky contacts.

The dominant role of surface effects on the control of MHL in the n-doped NW provides an opportunity to investigate the microscopic mechanism of carrier dynamics in III–V NWs. It is known that the high density of surface acceptor centers in bulk GaAs, up to $\sim 10^{12}$ cm^{-2}, will pin the Fermi level to 0.63–0.68 eV below the conduction band if filled by electrons.[29,30] For nanostructures, surface states with a density on the same order have been reported in InAs NWs.[42] Similar state can therefore be expected on the surface of wurtzite GaAs NWs, and the dense acceptor-like centers will be occupied by electrons depending on the doping condition. Taking a NW diameter of 100 nm, full occupation of surface states with density of 1×10^{12} cm^{-2} requires electron concentration above 4×10^{17} cm^{-3} and results in the same number of surface traps for minority holes. As schematically shown in Figure 9, for n-type doping below 1×10^{16} cm^{-3}, the NWs are fully depleted with a very low percentage of surface states (<5%) filled with electrons, thus yielding little influence on MHL. However, for 2×10^{17} cm^{-3} or higher level of n-type doping, on one hand, the negatively charged surface states with a density of $\geq 5 \times 10^{11}$ cm^{-2} will become the effective

recombination centers for photoinjected holes. On the other hand, the built-in field of $\sim 10^5$ V/cm in the radial direction will drive holes to accumulate on the surface of NWs. Both effects will cause a drop in MHL.

CONCLUSIONS

In conclusion, this study reveals the significant variation of photoresponsivity of vertically aligned wurtzite GaAs NWs with n-type doping. The minority hole lifetime of a single wire is obtained by the photoconductive characterization combined with numerical simulation. It is worthy to mention that the photoinjected carrier density is estimated to below 10^{14} cm^{-3} in our experiment, 3 orders lower than that generally applied in the spectroscopic methods; thus this study provides a scheme to probe the carrier dynamics close to the working condition in photovoltaic devices with minimized perturbation on the electronic status of the NW surface. For doping concentration higher than 2×10^{17} cm^{-3}, the hole lifetime can be lower than 1 ps, leading to linear photoelectric behavior, which deviates from the conventional response observed in undoped and lightly doped NWs. The contribution of doping-induced bulk effects, like the possible defects in NWs, on the carrier recombination rate is evaluated as $\sim 10^{10}$ s^{-1}, while that of the surface recombination could be more than 1×10^{12} s^{-1}. According to our results, moderate n-type doping in III–V semiconductor NWs would not reach the expected effect of efficiently increasing the concentration of majority electrons, but will instead form a high density of negatively charged surface traps. These may be the critical factors in designing and fabricating high-performance electronic and photoelectric devices based on NWs.

METHODS

Nanowire Growth and Sample Preparation. All GaAs NW samples were grown in a Riber 32 MBE system on GaAs (111)B-oriented semi-insulating substrates with silicon as the n-type dopant. Heavily n-doped buffer layer was grown to ensure the bottom electrical contact of NWs before the deposition of Au catalyst. The growth of GaAs NWs was at 500 °C with a V/III flux ratio of 20:1. For the three n-doped NW samples, the source temperature of Si was set as 875, 990, and 1025 °C corresponding to the nominal concentration of 1×10^{16}, 2×10^{17}, and 6×10^{17} cm^{-3} in NWs, respectively. For the GaAs/AlGaAs/GaAs core–shell NW, following growth of the GaAs core, the temperature is raised to 550 °C, and a nominally 15% AlGaAs shell ~30 nm thick is grown. After that, the outermost shell of ~5 nm GaAs is grown to prevent the oxidation of AlGaAs shell.[5,20,23] For the 2×10^{17} cm^{-3} n-doped core–shell NW, the silicon doping is just performed in the GaAs core, and the doping condition is the same as that of bare GaAs NWs. According to the relevant work on InAs NWs, the electron concentration increases linearly along with the partial pressure of the silicon dopant.[43] In our case, the forward conductivity of tip–wire Schottky contact increases with the rising doping level, indicating the stepwise n-type concentrations in NWs of the four samples. The experimental results are shown in the Supporting Information. Poly(methyl methacrylate) (PMMA) was selected to embed and support the GaAs NWs for C-AFM study. The samples were first spin-coated by PMMA with NWs fully buried. The polymer was then solidified by baking. Finally, the top surface of the NWs will be exposed for measurement by polishing, and the height of the remaining segment is about 5 μm, as shown in the inset of Figure 1b.

Photoconductive Measurement of Individual NWs. Conductive atomic force microscopy in a Multimode Nanoscope *IV* microscope was applied to characterize the NW's electrical properties with its utility described earlier.[32,33] Si probes coated with conductive diamond film were used for durable and repeatable measuring. The bias voltage was applied to the bottom electrode of a sample, while the tip was kept at virtual ground during the measurements. Individual NWs were identified by the electrical difference between wires and PMMA. An external 808 nm semiconductor laser was used to excite the GaAs NWs with the internal AFM laser (670 nm) spot placed away from the front end of the probe's cantilever to minimize the stray light excitation.[34]

As shown in Figure 3, the responsivity of an individual NW is normalized based on the formula below:

$$R_s = \frac{I_{ps} - I_{ds}}{P} \tag{4}$$

where R_s is the photoresponsivity of a single NW, I_{ps} is the current of a single NW under the illumination of the external 808 nm laser with intensity P, and I_{ds} is the background current of a single NW without intentional excitation which includes the leakage current of Schottky contact and the photocurrent excited by the AFM stray light (see Figure S2 in Supporting Information).

Structural and Photoluminescent Characterization. The morphological and structural characteristics of grown NWs were investigated by SEM (FEI Sirion 200, operated at 20 kV) and TEM (Philips Tecnai F20, operated at 200 kV). For TEM investigations, individual NWs were removed from the substrates using ultrasonic and deposited on the holey carbon supporting films.

Steady-state and time-resolved photoluminescence of an ensemble of NWs was obtained using pulsed 300 fs, 522 nm excitation. A helium-flow cryostat held the samples at 4.5 K, and the luminescence was measured using either a peltier-cooled CCD (steady-state) or a silicon single-photon avalanche photodiode (time-resolved luminescence) for time-correlated single photon counting, respectively. The resultant data were fit by convolution of an exponential decay with the instrument response function of the system—a response time of around 48 ps was measured.

Numerical Simulation. To simulate the photoconductive properties of the tip–NW setup, a two-dimentional model was established with SENTAURUS TCAD, a commercial package by Synopsys. The influence of silicon dopants on the dynamic and kinetic properties of photocarriers are included in the simulation under the schemes of Shockley–Read–Hall (SRH) recombination and mobility degradation by impurity scattering, respectively. Also, the effect of sidewall Fermi level pinning on the radial built-in electrical field within finite size is taken into account by setting fixed charges on the nanowire surface. Meanwhile, it is assumed that the undetermined impacts upon the carrier dynamics by n-type doping, including those of the contamination, defects in the NW and on its surface, can be involved in the effective recombination lifetime during simulation.

For the calculation of the basic transport properties of the NW, the drift-diffusion transport model is adopted, in which the distributions of electric potential and current density in NWs can be derived by solving the coupled Poisson, electron and hole continuity equations.

$$\nabla \varepsilon \cdot \nabla \psi = -q(p - n + N_{D^+} - N_{A^-}) \tag{5}$$

$$\vec{J}_n = -nq\mu_n \nabla \phi_n \tag{6}$$

$$\vec{J}_p = -pq\mu_p \nabla \phi_p \tag{7}$$

where ε is the electrical permittivity, ψ is the electric potential, q is the elementary electronic charge, n and p are the electron and hole densities, N_D+ is the number of ionized donors, N_A^- is the number of ionized acceptors, $\vec{J}_n$, $\vec{J}_p$, μ_n, μ_p, ϕ_n, and ϕ_p are the

current densities, mobilities, and quasi-Fermi potentials of electrons and holes. The impurity is assumed to be fully ionized, and the doping-dependent mobility degradation due to ionized impurity scattering is introduced. Taking into account the experimental low doping and photoinjection level of NW, Boltzmann statistics are assumed and the electron and hole concentrations can be computed from the electron and hole quasi-Fermi potentials.

Under illumination, the photogeneration rate of electron and hole pairs is simulated by the raytracing model.[44] For the tip−NW Schottky contact, the thermionic emission and tunneling effect were considered to calculate the current; the barrier height was decided to be 0.4−0.65 eV for different doping levels by fitting the *I*−*V* curves without intentional excitation, which is close to the reported value.[45]

With other parameters set as that of bulk GaAs, two parameters were adjusted to quantitatively fit the experimental photocurrent curves: the excitation intensity, which decides the magnitude of photocurrent, and the hole lifetime, the primary parameter to determine the increasing tendency of photocurrent against bias voltage. As shown in Figure 10, the hole lifetime in individual NWs can then be extracted from fitting with uncertainty less than ±30% for both saturated and linear photoconductive responses.

It is worthwhile to outline the applicable range of simulating the carrier lifetime from the photoelectric behavior. As discussed in the context related to Figure 6, the fitting is based on the bias-dependent L_D/L_p, namely, the relative increment of depletion length of Schottky barrier against the diffusion length of minority carrier. Thus the method is relatively accurate in deciding the hole lifetime with high $\Delta L_D(V)/L_p$, for instance, the system with low diffusion length as in the doped wires studied here. On the other hand, it will be less effective when the drift of carriers starts to dominate the photocurrent since the impact of carrier lifetime on the photo-*IV* will be weakened. Consequently, the method is unavailable in the case that the NW is fully depleted by a high reverse bias voltage.

Conflict of Interest: The authors declare no competing financial interest.

Acknowledgment. The authors acknowledge financial support from the National Basic Research Program of China (No. 2011CB925604), the National Science Foundation of China (Nos. 91121009, 91021015, 10604059, and 61006090), the Shanghai Basic Research Program (No. 09DJ1400101), and the Australian Research Council. H.X. and T.X.L. appreciate James Torley from University of Colorado at Colorado Springs for critical reading of the manuscript.

Supporting Information Available: The TEM images of GaAs NWs with different doping concentrations; the *IV* curves of GaAs NWs with different doping concentrations without external excitation; and the discrepancy of the carrier lifetime among NWs. This material is available free of charge *via* the Internet at http://pubs.acs.org.

REFERENCES AND NOTES

1. Kim, C. J.; Lee, H. S.; Cho, Y. J.; Kang, K.; Jo, M. H. Diameter-Dependent Internal Gain in Ohmic Ge Nanowire Photodetectors. *Nano Lett.* **2010**, *10*, 2043–2048.
2. Liu, K.; Sakurai, M.; Liao, M.; Aono, M. Giant Improvement of the Performance of ZnO Nanowire Photodetectors by Au Nanoparticles. *J. Phys. Chem. C* **2010**, *114*, 19835–19839.
3. Yan, C.; Singh, N.; Cai, H.; Gan, C. L.; Lee, P. S. Network-Enhanced Photoresponse Time of Ge Nanowire Photodetectors. *ACS Appl. Mater. Interfaces* **2010**, *2*, 1794–1797.
4. Soci, C.; Zhang, A.; Xiang, B.; Dayeh, S. A.; Aplin, D. P. R.; Park, J.; Bao, X. Y.; Lo, Y. H.; Wang, D. ZnO Nanowire UV Photodetectors with High Internal Gain. *Nano Lett.* **2007**, *7*, 1003–1009.
5. Gallo, E. M.; Chen, G. N.; Currie, M.; McGuckin, T.; Prete, P.; Lovergine, N.; Nabet, B.; Spanier, J. E. Picosecond Response Times in GaAs/AlGaAs Core/Shell Nanowire-Based Photodetectors. *Appl. Phys. Lett.* **2011**, *98*, 241113.
6. Dong, Y. J.; Tian, B. Z.; Kempa, T. J.; Lieber, C. M. Coaxial Group III Nitride Nanowire Photovoltaics. *Nano Lett.* **2009**, *9*, 2183–2187.
7. Tian, B. Z.; Zheng, X. L.; Kempa, T. J.; Fang, Y.; Yu, N. F.; Yu, G. H.; Huang, J. L.; Lieber, C. M. Coaxial Silicon Nanowires as Solar Cells and Nanoelectronic Power Sources. *Naure* **2007**, *449*, 885–889.
8. Kempa, T. J.; Tian, B. Z.; Kim, D. R.; Hu, J. S.; Zheng, X. L.; Lieber, C. M. Single and Tandem Axial p-i-n Nanowire Photovoltaic Devices. *Nano Lett.* **2008**, *8*, 3456–3460.
9. Tian, B. Z.; Kempa, T. J.; Lieber, C. M. Single Nanowire Photovoltaics. *Chem. Soc. Rev.* **2009**, *38*, 16–24.
10. Soci, C.; Zhang, A.; Bao, X. Y.; Kim, H. K.; Lo, Y.; Wang, D. L. Nanowire Photodetectors. *J. Nanosci. Nanotechnol.* **2010**, *10*, 1–20.
11. Shao, Y.; Yang, Y. Efficient Organic Heterojunction Photovoltaic Cells Based on Triplet Materials. *Adv. Mater.* **2005**, *17*, 2841–2844.
12. Wen, L.; Zhao, Z. F.; Li, X. H.; Shen, Y. F.; Guo, H. M.; Wang, Y. Q. Theoretical Analysis and Modeling of Light Trapping in High Efficicency GaAs Nanowire Array Solar Cells. *Appl. Phys. Lett.* **2011**, *99*, 143116.
13. Hu, L.; Chen, G. Analysis of Optical Absorption in Silicon Nanowire Arrays for Photovoltaic Applications. *Nano Lett.* **2007**, *7*, 3249–3252.
14. Zhang, A.; You, S. F.; Soci, C.; Liu, Y. S.; Wang, D. L.; Lo, Y. H. Silicon Nanowire Detectors Showing Phototransistive Gain. *Appl. Phys. Lett.* **2008**, *93*, 121110.
15. Parkinson, P.; Hughes, J. L.; Gao, Q.; Tan, H. H.; Jagadish, C.; Johnston, M. B.; Herz, L. M. Transient Terahertz Conductivity of GaAs Nanowires. *Nano Lett.* **2007**, *7*, 2162–2165.
16. Schroer, M. D.; Petta, J. R. Correlating the Nanostructure and Electronic Properties of InAs Nanowires. *Nano Lett.* **2010**, *10*, 1618–1622.
17. Jiang, X. C.; Xiong, Q. H.; Nam, S.; Qian, F.; Li, Y.; Lieber, C. M. InAs/InP Radial Nanowire Heterostructures as High Electron Mobility Devices. *Nano Lett.* **2007**, *7*, 3214–3218.
18. Fickenscher, M. A.; Jackson, H. E.; Smith, L. M.; Yarrison-Rice, J. M.; Kang, J. H.; Paiman, S.; Gao, Q.; Tan, H. H.; Jagadish, C. Direct Imaging of the Spatial Diffusion of Excitons in Single Semiconductor Nanowires. *Appl. Phys. Lett.* **2011**, *99*, 263110.
19. Jung, Y.; Vacic, A.; Perea, D. E.; Picraux, S. T.; Reed, M. A. Minority Carrier Lifetimes and Surface Effects in VLS-Grown Axial p−n Junction Silicon Nanowires. *Adv. Mater.* **2011**, *23*, 4306–4311.
20. Demichel, O.; Heiss, M.; Bleuse, J.; Mariette, H.; Fontcuberta i Morral, A. Impact of Surfaces on the Optical Properties of GaAs Nanowires. *Appl. Phys. Lett.* **2010**, *97*, 201907.
21. Léonard, F.; Talin, A. A.; Swartzentruber, B. S.; Picraux, S. T. Diameter-Dependent Electronic Transport Properties of Au-Catalyst/Ge-Nanowire Schottky Diodes. *Phys. Rev. Lett.* **2009**, *102*, 106805.
22. Parkinson, P.; Joyce, H. J.; Gao, Q.; Tan, H. H.; Zhang, X.; Zou, J.; Jagadish, C.; Herz, L. M.; Johnston, M. B. Carrier Lifetime and Mobility Enhancement in Nearly Defect-Free Core Shell Nanowires Measured Using Time-Resolved Terahertz Spectroscopy. *Nano Lett.* **2009**, *9*, 3349–3353.
23. Perera, S.; Fickenscher, M. A.; Jackson, H. E.; Smith, L. M.; Yarrison-Rice, J. M.; Joyce, H. J.; Gao, Q.; Tan, H. H.; Jagadish, C.; Zhang, X.; *et al.* Nearly Intrinsic Exciton Lifetimes in Single Twin-Free GaAs/AlGaAs Core−Shell Nanowire Heterostructures. *Appl. Phys. Lett.* **2008**, *93*, 053110.
24. Zhang, A.; Kim, H.; Cheng, J.; Lo, Y. Ultrahigh Responsivity Visible and Infrared Detection Using Silicon Nanowire Phototransistors. *Nano Lett.* **2010**, *10*, 2117–2120.
25. Chen, M. T.; Lu, M. P.; Wu, Y. J.; Song, J. H.; Lee, C. Y.; Lu, M. Y.; Chang, Y. C.; Chou, L. J.; Wang, Z. L.; Chen, L. J. Near UV LEDs Made with *In Situ* Doped p−n Homojunction ZnO Nanowire Arrays. *Nano Lett.* **2010**, *10*, 4387–4393.
26. Li, J.; Zhang, Y.; To, S.; You, L. D.; Sun, Y. Effect of Nanowire Number, Diameter, and Doping Density on Nano-FET Biosensor Sensitivity. *ACS Nano* **2011**, *5*, 6661–6668.

27. Perea, D. E.; Hemesath, E. R.; Schwalbach, E. J.; Lensch-Falk, J. L.; Voorhees, P. W.; Lauhon, L. J. Direct Measurement of Dopant Distribution in an Individual Vapour–Liquid–Solid Nanowire. *Nat. Nanotechnol.* **2009**, *4*, 315–319.
28. Cui, Y.; Lieber, C. M. Functional Nanoscale Electronic Devices Assembled Using Silicon Nanowire Building Blocks. *Science* **2001**, *291*, 821–853.
29. Filipavičius, V.; Gaidys, R.; Matulaitis, V. A.; Petrauskas, G.; Sakalas, A.; Sakalauskas, S. Investigation of the Surface States in Heavily Doped GaAs by Kelvin Probe. *Phys. Status Solidi A* **1987**, *99*, 543–547.
30. Walther, C.; Blum, R. P.; Niehus, H.; Masselink, W. T. Modification of the Fermi-Level Pinning of GaAs Surfaces through InAs Quantum Dots. *Phys. Rev. B* **1999**, *60*, R13962–R13965.
31. Colombo, C.; Heiss, M.; Gratzel, M.; Fontcuberta i Morral, A. Gallium Arsenide p-i-n Radial Structures for Photovoltaic Applications. *Appl. Phys. Lett.* **2009**, *94*, 173108.
32. Park, W. I.; Yi, G. C.; Kim, J. W.; Park, S. M. Schottky Nanocontacts on ZnO Nanorod Arrays. *Appl. Phys. Lett.* **2003**, *82*, 4358–4360.
33. Fan, Z. Y.; Dutta, D.; Chien, C. J.; Chen, H. Y.; Brown, E. C.; Chang, P. C.; Lu, J. G. Electrical and Photoconductive Properties of Vertical ZnO Nanowires in High Density Arrays. *Appl. Phys. Lett.* **2006**, *89*, 213110.
34. Yin, H.; Li, T. X.; Wang, W. J.; Hu, W. D.; Lin, L.; Lu, W. Scanning Capacitance Microscopy Investigation on InGaAs/InP Avalanche Photodiode Structures: Light-Induced Polarity Reversal. *Appl. Phys. Lett.* **2009**, *95*, 093506.
35. Gao, W.; Berger, P. R.; Zydzik, G. J.; O'Bryan, H. M.; Sivco, D. L.; Cho, A. Y. $In_{0.53}Ga_{0.47}As$ MSM Photodiodes with Transparent CTO Schottky Contacts and Digital Superlattice Grading. *IEEE Trans. Electron Devices* **1997**, *40*, 2174–2179.
36. Chen, G. N.; Gallo, E. M.; Burger, J.; Nabet, B.; Cola, A.; Prete, P.; Lovergine, N.; Spanier, J. E. On Direct-Writing Methods for Electrically Contacting GaAs and Ge Nanowire Devices. *Appl. Phys. Lett.* **2010**, *96*, 223107.
37. Yamashita, T.; Akiyama, T.; Nakamura, K.; Ito, T. Effects of Facet Orientation on Relative Stability between Zinc Blende and Wurtzite Structures in Group III–V Nanowires. *Jpn. J. Appl. Phys.* **2010**, *49*, 055003.
38. Akiyama, T.; Nakamura, K.; Ito, T. Structural Stability and Electronic Structures of InP Nanowires: Role of Surface Dangling Bonds on Nanowire Facets. *Phys. Rev. B* **2006**, *73*, 235308.
39. Cahangirov, S.; Ciraci, S. First-Principles Study of GaAs Nanowires. *Phys. Rev. B* **2009**, *79*, 165118.
40. Sinning, S.; Dekorsy, T.; Helm, M.; Mussler, G.; Däweritz, L.; Ploog, K. H. Reduced Subpicosecond Electron Relaxation in GaN_xAs_{1-x}. *Appl. Phys. Lett.* **2005**, *86*, 161912.
41. Kumakura, K.; Makimoto, T.; Kobayashi, N.; Hashizume, T.; Fukui, T.; Hasegawa, H. Minority Carrier Diffusion Length in GaN: Dislocation Density and Doping Concentration Dependence. *Appl. Phys. Lett.* **2005**, *86*, 052105.
42. Salfi, J.; Paradiso, N.; Roddaro, S.; Heun, S.; Nair, S. V.; Savelyev, I. G.; Blumin, M.; Beltram, F.; Ruda, H. E. Probing the Gate-Voltage-Dependent Surface Potential of Individual InAs Nanowires Using Random Telegraph Signals. *ACS Nano* **2011**, *5*, 2191–2199.
43. Wirths, S.; Weis, K.; Winden, A.; Sladek, K.; Volk, C.; Alagha, S.; Weirich, T. E.; von der Ahe, M.; Hardtdegen, H.; Lüth, H.; *et al.* Effect of Si-Doping on InAs Nanowire Transport and Morphology. *J. Appl. Phys.* **2011**, *110*, 053709.
44. *DESSIS ISE TCAD Manual*, release 10.06; ISE Integrated Systems Engineering AG: Zurich, 2005.
45. Hu, J.; Saraswat, K. C.; Philip Wong, H. S. Metal/III–V Schottky Barrier Height Tuning for the Design of Non-alloyed III–V Field-Effect Transistor Source/Drain Contacts. *J. Appl. Phys.* **2010**, *107*, 063712.